State Estimation for Shore Monitoring Using an Autonomous Surface Vessel

Gregory Hitz, François Pomerleau, Francis Colas, Roland Siegwart

State Estimation for Shore Monitoring Using an Autonomous Surface Vessel

Gregory Hitz[1], François Pomerleau[1,2], Francis Colas[1], and Roland Siegwart[1]

[1] ETH Zurich, Autonomous Systems Lab, 8092 Zurich, Switzerland.
[2] Université Laval, Département d'informatique et de génie logiciel, QC, Canada

Abstract. Although many applications of small Autonomous Surface Vessels rely on two-dimensional state estimation, inspection tasks based on long-range sensors require more accurate attitude estimates. In the context of shoreline monitoring relying on a nodding laser scanner, we evaluate three different extended Kalman filter approaches with respect to an accurate ground truth in the range of millimeters. Our experimental setup allowed us to track the impact of sensors noise, including GPS non-Gaussian error, a phenomenon often underestimated. Extensive field experiments demonstrate that the use of a complementary filter in combination with a model-based extended Kalman filter performed best and reduced velocity errors by 73% compared to GPS. Finally, following our state estimation observations, we present a long-term shore monitoring result highlighting changes in the environment over a period of 6 months.

Keywords: State Estimation, ASV, ICP, Shore Monitoring, 3D Point Clouds

1 Introduction

Most of the small and medium Autonomous Surface Vessels (ASVs), like the one presented in Fig. 1, operate in open environments and handle many tasks, such as station keeping [17], path following [1], or environmental monitoring [7, 8]. Those researches demonstrated that a low precision two-dimensional (2D) state estimation based on GPS and compass measurements is sufficient for such applications. Unfortunately, other applications, such as mapping shorelines [20] or bathymetry [3], rely on long-range sensors. Such applications are sensitive to poor attitude estimation leading to noise often referred to as motion blur. For example, many three-dimensional (3D) scanners used in robotics are assembled from a 2D laser rangefinder and a motor. This type of scanner takes approximately 2 seconds to complete a swipe. During this time, the ASV rocks with the waves and, even at low speed, can change position significantly. To give an idea of the distortion, a typical 5° oscillation of the boat causes more than a meter vertical uncertainty on the localization of a feature at a distance of 10 m, leading to significant motion blur in the resulting point clouds. There are ways to circumvent the problem of attitude estimation. Increasing the acquisition rate by ensuring a fast shutter speed of cameras can be achieved by using the platform

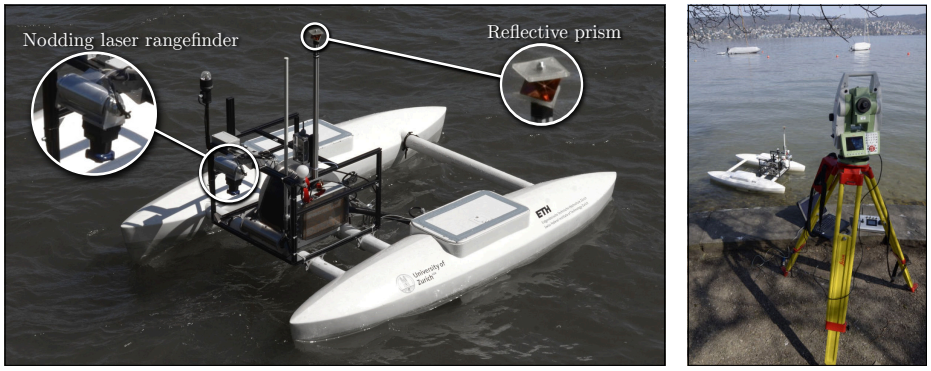

Fig. 1: *Left*: Our ASV, equipped with a reflective prism and a nodding laser scanner. *Right*: The theodolite (Leica Total Station TS15), used for ground truth measurements, positioned on shore.

in bright daylight [4]. Also, high-end laser rangefinders allowing high scanning frequency can be used [16], increasing significantly the cost of the platform. Finally, the attitude problem can be directly addressed at the design level by implementing passive damping systems [10] or by increasing the size and inertia of the ASV. Such systems can reduce the impact of the main motion frequency, but can hardly be built generic enough to handle the large spectrum of events that an ASV can encounter during a mission. To overcome those limitations, we investigate how attitude estimation can be added in a 3D state estimation algorithm fulfilling properly the constraints of an ASV.

Solutions for 3D state estimation were widely investigated in the recent years. Developed in the context of large ocean vehicles, Fossen [6] proposed a more traditional approach using a dynamic system model to feed as prediction to an extended Kalman filter (EKF), while all the sensors are used in the correction step. Motion models linking the commands to states can be difficult to build or computationally expensive to compute. This is particularly true for the the Unmanned Aerial Vehicle (UAV) field. To overcome this problem, EKFs using the Inertia Measurement Unit (IMU) directly in the prediction step were proposed [12]. Focussing only on the attitude estimation based on an IMU, Mahony et al. [13] introduced the concept of the Complementary filter (CF) and demonstrated its performance on a micro aerial vehicle. This variety of solutions require a deeper investigation on how the IMU should be used in an EKF. Moreover, those solutions were not developed for ASVs, which have their own motion characteristics. To adopt the proper solution, we compare the current state-of-the-art EKF algorithms using an external tracking system which provides us with highly accurate ground truth measurements and discuss the impact of the ASV particularities on those filters.

Finally, range measurements can be used to monitor shoreline vegetation, but can also facilitate an additional localization method for the ASV. The registration of subsequent point clouds provides relative position updates and, a step

further, the comparison against a known map links the position information to a global frame. Rectifying laser scan measurements via state prediction during the swiping has been done for other types of robots (e.g. ground robots [11] and quadrotors [15]). Another approach is to include the laser information directly in the state estimation [2]. This solution works well when the surrounding environment constrains properly the scan registration, but sensor maximum range coupled with water reflectivity can reduce the returned points to an unstable number. Shoreline monitoring has been shown to be a delicate operation for the integrity of the platform when using a quadrotor [20]. ASVs can support large payloads and repeatedly navigate in a given area. As reported by Kelly et al. [9], experiments aiming at long-term autonomy require a higher level of integration than short term experiments. This might explain why, to the knowledge of the authors, no prior work on shore monitoring was presented. Thus, we conclude our paper by presenting 3D mapping results highlighting environmental changes that occur over a period of 6 months. Map management techniques allow us to maintain a clean representation of the environment, while being able to adapt to changes. The ASV used for the paper is shown in Fig. 1, with the up and down nodding Hokuyo laser in front. The other sensors are a GPS receiver, a compass and an IMU. The boat measures 2.5 x 1.8 x 0.9 m and weighs approximately 155 kg. It is used as a toxic cyanobacteria monitoring tool and is fully described in [8].

2 State Estimation for ASVs

The goal of using state estimation procedures is to estimate the state of a system more accurately, given measurements from a set of sensors. In our application, we want to estimate the position and attitude of the body fixed frame $\{B\}$ with respect to an inertial world frame $\{W\}$. For this purpose, we use an EKF, which makes use of a prediction model to assess how probable measurements are when they are fed to the filter. The basis of Kalman filter (KF) will be considered as textbook knowledge for the purpose of this article, so we will only describe the specificities of the filter variants we investigated in this section.

In our application, there are three sensors which provide data to the filter. The GPS receiver measures the position of the boat with respect to the world frame. The compass (in our case, a one-dimensional one) provides the north vector in the body frame. Furthermore, the IMU measures the accelerations and the angular velocities of the body in the body frame. We assume that all our sensor measurements are corrupted by additive white Gaussian noise. We also assume that the accelerometers and gyroscopes of the IMU are distorted by time varying, additive biases, which need to be estimated along with the states of the system. Assuming that GPS measurements are only affected by white Gaussian noise is problematic, yet greatly simplifies the mathematical description. We will discuss this issue in the results section.

The world frame $\{W\}$ is defined as a metric North-East-Down frame (NED). In our specific case, we use the Swiss grid [5], which is based on a Mercator

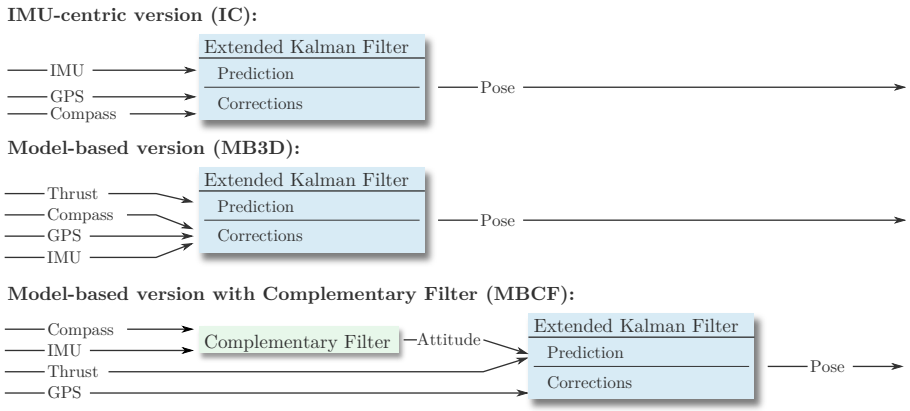

Fig. 2: The three filtering schemes used for state estimation. From top to bottom: IC, MB3D and MBCF.

projection. However, any other metric coordinates could be used (e.g. UTM). We directly convert GPS measurements from WGS84 to Swiss grid coordinates before feeding them to the state estimator. The body frame of the boat is defined similarly to the world frame with the x axis pointing forwards, the y axis to the right and z downwards. In the following, we describe three different formulations of EKFs to perform state estimation on our ASV. Fig. 2 gives an overview of the three filter versions.

2.1 IMU-centric Extended Kalman Filter

The IMU-centric filter implements the state-of-the-art EKF formulation that is mostly used in UAV applications. It is favored for complex systems since it circumvents the use of dynamical models by directly integrating the IMU measurements in the prediction steps, treating them as a system input rather than actual sensor measurements. This simplifies the prediction model to simple kinematic equations. The measurements from the GPS receiver and the compass are treated as regular updates in the EKF. Our formulation of the IMU-centric EKF follows closely the one of Leutenegger and Siegwart [12]. The state vector is defined as $x = [p, q, v, b_g, b_a]^{\mathrm{T}}$ where $p \in \mathbb{R}^3$ defines the position in the world frame, $q \in SO(3)$ is a unit quaternion describing the attitude, $v \in \mathbb{R}^3$ is the linear velocity of the boat in the world frame, $b_g \in \mathbb{R}^3$ and $b_a \in \mathbb{R}^3$ describe the biases of the gyroscopes and accelerometers respectively. The covariance matrix of the quaternion representing the attitude is not well defined due to its unit length constraint [21]. Therefore, the filter is defined to operate on the error state. For the attitude it is defined multiplicative: $\hat{q} = \delta q \otimes q$, whereas for the other states it is additive: $\hat{x}_{\backslash q} = x_{\backslash q} + \Delta x_{\backslash q}$. The resulting error quaternion δq can be reduced to a 3D representation using small angle approximations [21], which renders the covariance matrix non-singular again. The full derivation of

the update equations and Jacobian matrix are not provided here, but follow closely the ones provided by Leutenegger and Siegwart [12].

2.2 Model-based Extended Kalman Filter

The model-based EKF implementation uses a dynamic model, which describes the dynamics of the system based on the commands sent to the motors. For the derivation of the model, we follow the work of Fossen [6]. The model is defined by a kinematic part (Eq. 1) and a dynamic part (Eq. 2):

$$\dot{\eta} = J(\eta)\nu \tag{1}$$

$$M\dot{\nu} + C(\nu)\nu + D(\nu)\nu + g(\eta) = \tau_m + \tau_e \tag{2}$$

where $\eta \in \mathbb{R}^6$ is the position and attitude of the boat defined in the world frame $\{W\}$, $\nu \in \mathbb{R}^6$ its linear and rotational velocities in the body frame $\{B\}$, M the inertia matrix, C the Coriolis matrix, D the damping matrix, g a vector of hydrostatic restoring forces, τ_m the thruster forces as input and τ_e unknown external perturbations. For this model, we use a set of Euler angles to represent the attitude of the boat, which simplifies the modeling of the hydrodynamic restoring forces. Note that the well-known singularity at 90° pitch is not problematic for a surface vessel. We formulate the model (Eq. 2) around the center of gravity of the body. Therefore, the inertia matrix can be formulated as follows:

$$M = \begin{bmatrix} m\,\mathbb{I}_{3\times3} & 0_{3\times3} \\ 0_{3\times3} & I_g \end{bmatrix}$$

where m is the mass of the boat, $\mathbb{I}_{3\times3}$ is the 3×3 identity matrix, and $I_g \in \mathbb{R}^{3\times3}$ is the rotational inertia matrix. To further simplify the model and reduce the number of parameters, we assume that $I_g = \mathrm{diag}(I_x, I_y, I_z)$.

The Coriolis matrix is defined as follows:

$$C(\nu) = \begin{bmatrix} mS(\nu_2) & 0_{3\times3} \\ 0_{3\times3} & -S(I_g\nu_2) \end{bmatrix}, \quad \text{where} \quad S(x) = \begin{bmatrix} 0 & -x_3 & x_2 \\ x_3 & 0 & -x_1 \\ -x_2 & x_1 & 0 \end{bmatrix} \tag{3}$$

$\nu_2 \in \mathbb{R}^3$ denotes the rotational part of ν and $S(x)$ denotes the cross-product operator.

Simple linear damping forces have proven to yield good results, at least in the velocity regimes that our ASV operates in (i.e. up to 1.5 m/s). Therefore, we use the following damping matrix:

$$D(\nu) = \mathrm{diag}(D_x, D_y, D_z, D_\phi, D_\theta, D_\psi)$$

The hydrostatic restoring forces are most difficult to model. The buoyancy of a vessel is defined by the mass of water that it displaces, which depends on the (unknown) shape of the the local water surface surrounding the boat. Even when assuming a flat water surface, the buoyancy depends on the geometry of the

boat. While the geometry is usually known, it is less straightforward to define the derivatives thereof, which are necessary to formulate the Jacobian matrix of the entire system. Fossen [6] has derived a simplified formulation under the assumptions of small roll and pitch angles and box-shaped vessels. It decouples the different dimensions and results in a linear equations:

$$g(\eta) = G\eta \quad \text{where} \quad G = \text{diag}(0, 0, G_z, G_\phi, G_\theta, 0) \tag{4}$$

Using this simplification the resulting dynamics are described by linear second order systems.

The state vector for the filter is defined as $x = [\eta^T, \nu^T, b_g]^T$ and is discretized at constant time intervals Δt. The discretized state transition and the Jacobian matrix are then defined as follows:

$$x_{k+1} = x_k + \Delta t\, \dot{x}_k \qquad\qquad F = \frac{\partial x_{k+1}}{\partial x_k} = I + \Delta t \frac{\partial \dot{x}_k}{\partial x_k}$$

The Jacobian matrix can be computed analytically. Due to space restrictions we have to omit this derivation here. While the updates of compass, GPS and gyroscope measurements are straightforward, the measured accelerations can not be used directly. In the general case, the IMU is not situated in the center of gravity and thus the measured accelerations need to be translated to the center of gravity. Since this is done in a moving frame $\{B\}$, the translation depends not only on the rotational velocities, but also on the rotational accelerations. As this is unpractical, the other option would be to shift the center of the model equations to the IMU. This however, makes the model itself far more complicated. For these reasons we do not use the measured accelerations in the model-based version.

2.3 Attitude estimation with the Complementary Filter

In our third approach we use a separate estimator for the attitude of the ASV. For this purpose we use the Complementary filter (CF) [13], which integrates the gyroscopic measurements ω and corrects them with measurements of known directions v_i. The state of the filter consists of the attitude represented by a unit quaternion $\hat{q}$ and a vector of additive gyroscope biases $\hat{b}_g$. The CF is then defined as follows:

$$\begin{aligned}
\omega_c &= -\text{vex}\left(\sum_{i=1}^{N} \frac{k_i}{2}\left(v_i \hat{v}_i^T - \hat{v}_i v_i^T\right)\right) \\
\dot{\hat{q}} &= \frac{1}{2}\,\hat{q} \otimes \left(\omega - \hat{b}_g + k_P \omega_c\right) \\
\dot{\hat{b}}_g &= -k_I \omega_c
\end{aligned}$$

where $\text{vex}(\cdot)$ defines the inverse operator of the cross-product operator (Eq. 3): $\text{vex}(S(a)) = a$ for $a \in \mathbb{R}^3$. The correction term ω_c depends on the measured

directions v, on the estimates thereof $\hat{v}$ and on their respective weights k_i. k_P and k_I denote filter parameters. In our case, the measured directions are provided by the compass and the accelerometers. The compass measures the north vector and the accelerometers provide the direction of gravity. However, the gravity vector is affected by the accelerations, which are induced by the motors. Such distortions can be avoided by having the model described above estimate the forces caused by the motors and correct the measurements. Given the attitude estimate from the CF, we use a simplified version of the model-based state estimator to estimate the remaining states (positions p and linear velocities v).

2.4 Point cloud registration

Building upon the state estimation procedures presented above, we can assemble undistorted point clouds from the range measurements of the laser scanner. Using an optimized version of the Iterative Closest Point algorithm based on the observation of Pomerleau et al. [19], we register the point clouds to a global map. Furthermore, state-of-the-art map management methods [18] allow us to distinguish static and dynamic points. This brings several benefits. First, shorelines are usually not entirely static, for instance boats that are moored at a single buoy have different positions depending on wind conditions. Second, noisy points which are introduced by state estimation errors, are classified as dynamic points and can be removed. Finally, it allows to detect seasonal changes in the shoreline vegetation, which can be of interest for biological studies, one of the scientific goals of our ASV.

3 Experiment Setup

To evaluate the presented state estimation approaches, we conducted several series of field tests. We used the collected data to estimate model parameters and assess the noise level of the GPS receiver. We also collected shoreline mapping data sets with the laser rangefinder over the course of 6 months.

3.1 Ground truth positioning information

To go beyond comparing the results of the state estimation against its sensor input (GPS and compass measurements), we recorded ground truth positioning information with an external positioning device. For this purpose, we mounted a reflective prism on the boat (see Fig. 1), which was then tracked by a theodolite (Leica Total Station TS15). This device is able to track the prism in a range of up to 2 km with 2 mm accuracy. However, this only provides positioning ground truth and no information about the attitude of the boat. As Fig. 1 shows, the prism had to be mounted 116 cm above the center of gravity of the boat to ensure visibility at all times. Rocking motions of 5° lead thus to a horizontal offset of up to 0.1 m. Such errors can either be corrected by the attitude estimate (which might however also introduce additional errors), or be ignored since the error is still an order of magnitude smaller when compared to GPS noise.

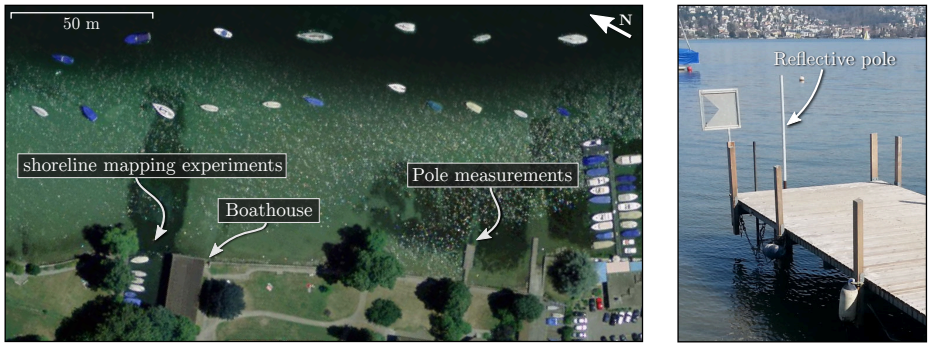

Fig. 3: *Left*: Overview of the testing area. Image source: Google Earth, 47.32023° N, 8.553017° E, Feb. 6, 2014. *Right*: The reflective pole used to assess the distortion of point clouds.

3.2 Point cloud distortion measure

Measuring the attitude of the ASV in a very precise manner is very difficult. One approach, which was used for work on rovers for lunar missions [14], would be to track three or more reference points on the boat simultaneously, creating a setup similar to indoor tracking systems. Having only one theodolite available rendered the use of external observation methods infeasible. The use of visual markers on shore and a camera on the boat could be a good solution, but the distance between the shore and the boat would reduce greatly the accuracy of those measurements. To circumvent this issue, we chose not to quantify the absolute attitude error, but rather the distortion of the resulting point clouds. For this purpose, we set up a specific experiment, referred to as *pole experiment* henceforth. A pole covered by reflective material was mounted on a pontoon (see Fig. 3) and was scanned repeatedly using the laser mounted on the boat. As the measured points on the pole have significantly higher return intensities, they can be extracted from the point cloud simply by applying a constant threshold. Fitting a line to the extracted points provides two measures which we have used to assess the distortion of the point cloud. First, the root mean squared error (RMSE) of the line fit provides a measure of distortion. Second, the deviation of the inclination of the fitted line from the vertical provides an additional performance measure. During this test, the boat was not actuated, i.e. only affected by waves. To eliminate distortion caused by linear motion of the boat, we used the theodolite to track the motion of the ASV during the test.

3.3 State estimation evaluation

In addition to the *pole experiment* described above, we have defined the following error metrics to evaluate the results of the three state estimation approaches.

$$e_{\text{pos},k} = \left\| p_k - p_{l,k} \right\|_2 \quad (5) \qquad d_{\text{pos},k} = \left\| p_{k+1} - p_k \right\|_2 \quad (7)$$

$$e_{\text{vel},k} = \left\| v_k - v_{l,k} \right\|_2 \quad (6) \qquad d_{\text{vel},k} = \left\| v_{k+1} - v_k \right\|_2 \quad (8)$$

$$d_{\text{att},k} = \left| \ln \left(q_{k+1} \otimes q_k^{-1} \right) \right| \quad (9)$$

where p_l and v_l refer to position and derived velocity measurements from the theodolite. The index k refers to the value at time step t_k. Equations 5 and 6 describe the error in position (e_{pos}) and velocity (e_{vel}). These are measured by computing the estimation error with respect to ground truth measurements and give thus an absolute error. To measure the smoothness of an estimated state trajectory, we use a measure of discontinuity d which is defined for position (d_{pos}), velocity (d_{vel}) and attitude (d_{att}) by the equations 7 to 9, respectively. Measuring smoothness reveals drastic update step which can occur whenever predicted measurements and actual sensor values do not match well in the update steps of the EKF.

4 Results

We have conducted a series of field experiments, during which we have collected data sets consisting of GPS, compass and IMU measurements, system specific information (such as thrust values of the motors) and external position information from a theodolite. We collected data in 5 one-day campaigns, during which the boat traveled an overall distance of 10.3 km. We encountered varying conditions ranging from strong winds and rain to very calm days, resulting in data sets with different environmental influences.

4.1 Model parameters

The proposed model-based state estimator relies on the underlying model of the ASV, which then is highly dependent on its parameters. Besides the weight of the boat, which we have measured with a spring scale (155 kg), there are several other parameters that can not be measured directly. To estimate them we have manually conducted an iterative optimization with respect to measured data. Table 1 provides an overview of those parameters.

Table 1: Parameters for the model of the ASV.

Damping		Inertia	Restoring forces
D_x: 80 kg s^{-1}	D_ϕ: 0.5 kg m^2 s^{-1}	I_ϕ: 5 kg m^2	G_ϕ: 70 kg m^2 s^{-2}
D_y: 1000 kg s^{-1}	D_θ: 0.5 kg m^2 s^{-1}	I_θ: 2 kg m^2	G_θ: 70 kg m^2 s^{-2}
D_z: 900 kg s^{-1}	D_ψ: 200 kg m^2 s^{-1}	I_ψ: 190 kg m^2	G_z: 600 kg s^{-2}

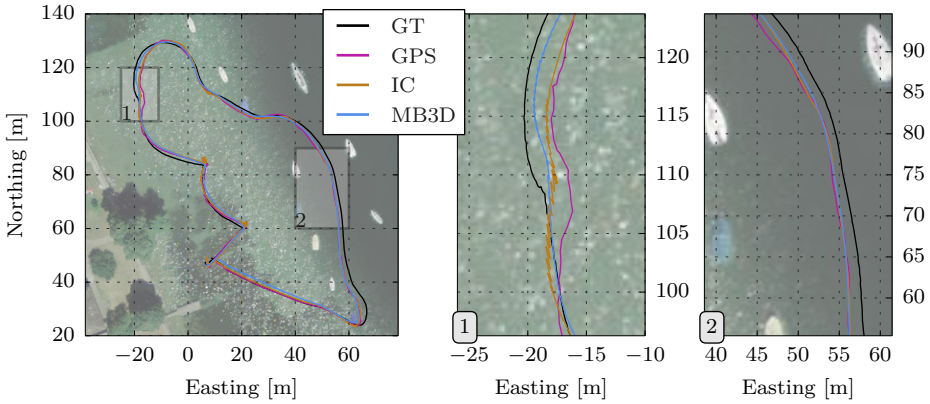

Fig. 4: *Left*: Top view of resulting trajectories. GT refers to the ground truth data from the theodolite (black line), IC denote the IMU-centric approach (brown line) and MB3D the model-based approach (blue line). The GPS measurement are represented with a purple line. *Middle and Right*: Zoomed results showing GPS offset.

4.2 State estimation

Fig. 4 shows both the raw GPS data points and the theodolite measurements (GT) along an example of a short round trip path. The graph clearly shows the limitations of the GPS measurements, with an average error of 1.9 m. However, the graph also shows that the error is not Gaussian, but rather shows constant offsets in a particular direction, which is highlighted in the first inset (1), where the GPS measurements start diverging severely from the ground truth. The third EKF version (MBCF) is not shown in Fig. 4, because it bases on the same motion model as MB3D and thus the resulting trajectory is almost identical. While the overview on the right shows that both versions follow the ground truth nicely, the two insets (1) and (2) show in more detail the errors caused by the GPS offsets: as the EKFs assume Gaussian noise on the GPS signal, they eventually drift to reduce the relative error to the GPS signal (see inset (1)). As long as the offset on the GPS signal remains relatively constant (see inset (2)), the estimates from both EKFs cannot reduce the error with respect to the ground truth. This is a common problem when using GPS signals and it emphasizes why we are interested in feeding exteroceptive measurements into the state estimators. As a result of this the overall performance of all EKF implementations in terms of the position error (Eq. 5) is only slightly better than the raw GPS positioning.

Fig. 5 shows the results of the evaluation according to the metrics defined in equations 5 to 9 of combined data from all 5 test days. For the absolute errors in position (a) and velocity (b) the raw GPS is provided as a comparison. In the case of the velocity, this refers to the differentiation of the GPS points. Since the discontinuity measures are not absolute, we can not compare them to the raw GPS input.

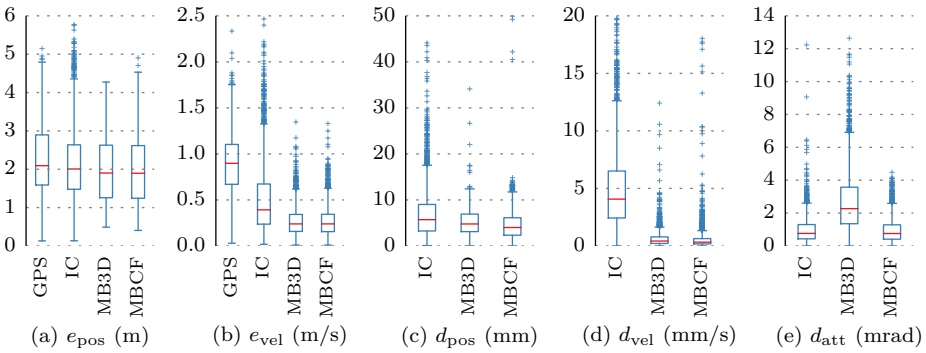

Fig. 5: Results of the evaluation. The metrics are: position error (e_{pos}), velocity error (e_{vel}), position discontinuity (d_{pos}), velocity discontinuity (d_{vel}), attitude discontinuity (d_{att}). For the first two, the raw GPS is shown as a baseline.

As already observed in the top view in Fig. 4, there is only very little improvement in terms of the absolute position error e_{pos} with respect to the raw GPS measurements. The medians reduced by 4.1%, 9.1% and 9.4% for the IC, MB3D and MBCF versions. While these differences are statistically significant[3], the difference between MB3D and MBCF is not ($p = 0.24$). This correlates with the fact that these two versions are based on the same model for linear motion and thus have very similar errors. The high position errors for all EKF versions highlight the problem of non-Gaussian GPS offsets. Whereas the positioning information can not be improved significantly, the estimates of the velocity clearly improve with respect to the GPS baseline. The model-based versions (MB3D and MBCF) show the lowest velocity errors (73.5% and 73.2% better than GPS). The IMU-centric EKF has still quite some outliers and only improves by 56.3% with respect to the baseline, which is due to wrong estimates of the accelerometer biases. Since the GPS measurements clearly have non-Gaussian components, the corresponding position updates map the error to the accelerometer biases and velocity estimates. This effect also leads to less smooth state trajectories in the position and velocity space. Figures 5(c) and 4(d) show this in terms of the discontinuity measure (cf. Eq. 7 - 9). A high discontinuity measure indicates that the corresponding state was frequently corrected, leading to large differences between two subsequent states. Wrong estimates of the accelerometer biases distort the velocity estimates during the predictions, which then need to be corrected by sensor updates. Especially the discontinuity of the velocity estimates shows that the model-based versions (MB3D and MBCF) result in smoother trajectories than the IC version.

The discontinuity of the attitude estimates suggests that MB3D has higher inconsistencies, which relates to the fact that it relies on a parameter-based, strongly simplified model. Even though we estimated these parameters with respect to field data, the linear formulation of the hydrostatic restoring forces

[3] We use the Mann-Whitney U test, with $p < 0.001$ as significance threshold.

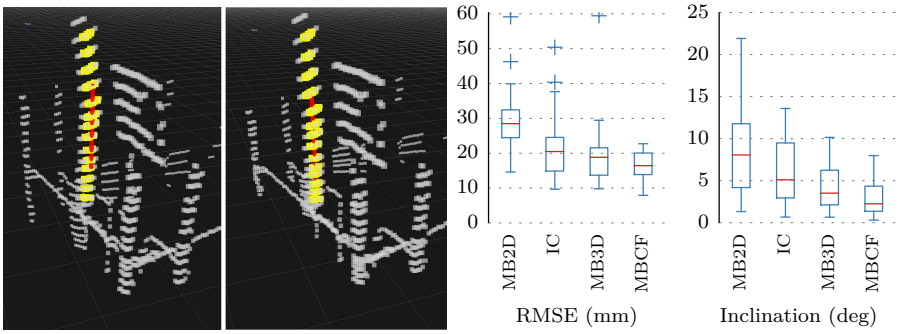

Fig. 6: Results of the pole experiment. *Left:* An example of an assembled point cloud without and with attitude estimation. The yellow points indicate the pole. The red line shows a 1 m segment of the fitted line. *Right:* The fitting errors and the resulting inclination of the fitted line. 46 point clouds were used.

(cf. Eq. 4) might be too simple to accurately describe the motion. In relation to the MB3D version, the IC and MBCF implementations have lower discontinuities (improvements by 66.4% and 66.7%). Both versions achieve relatively smooth attitude trajectories as they directly integrate the gyroscope measurements. Even though there are quite some difference in their implementations, the resulting distributions of discontinuity measures do not differ significantly (p=0.08).

Fig. 6 presents the results of the pole experiment. On the left hand side, an example of a distorted point cloud and its rectified version is shown. The pole that was used as a vertical and straight reference is highlighted in yellow in both pictures. To assemble the distorted point clouds as a baseline, the model-based state estimator was used in 2D, thus ignoring any roll and pitch. The images also show a 1 m segment of the fitted line in red. A total of 46 point clouds were processed, i. e. the pole was extracted in each point cloud and a line was fitted to it. The resulting statistics are shown on the right in Fig. 6. The RMSE of the fitted lines show that there is clearly most distortion in the baseline, where no attitude estimation is used. The MBCF version performs best, owing to its good model-based translational components and the direct integration of the gyroscope measurements in the complementary filter. A possible explanation for the poor performance of the IMU-centric implementation is that, also here, erroneous bias estimates distort the gravity vector. Those biases influence the final attitude estimates leading to a larger error. The inclination of the line also shows that the MBCF performs best. The inclination angles have the lowest median and the smallest spread, meaning that the fitted lines were most upright. One could note that the lack of a ground truth measurement of the poles inclination causes a few degrees of uncertainty in the inclination measure in an absolute sense, but the relative performances between solutions remain the same.

The experimental comparison of the three proposed state estimators showed that the model-based version in combination with a complementary filter (MBCF), performed best for the system at hand. It combined the good performance of the

linear components of the model-based approach, with the simplicity of the IMU-centric version for the attitude estimation. And thus, circumvented the need for formulating an accurate model of the hydrostatic restoring forces, which describe the rocking motion of the boat. Our results also show that the IMU-centric version does not perform as well as one might expect, which is mostly due to the error on the GPS signal. In comparison to the work of [12], the motion of an ASV is in the same order of magnitude as the error level on the GPS readings. This fact and the non-Gaussian characteristics of the noise lead to a lower performance when applied on an ASV.

4.3 Point cloud mapping

As it was our goal to collect point cloud information of shoreline areas, we have also collected a data set consisting of laser scans, GPS, compass and IMU measurements during a period of four months from October 10, 2013 to April 16, 2014. Different weather conditions were encountered, such as rain, bright sunlight, moderate wind and consequently waves. Fig. 7 shows the final map on the left and gives a qualitative assessment of the achieved accuracy. The boathouse has straight and sharp walls and consistent rectangular corners. The map also shows large trees in the back of the small harbor, which can cause severe GPS shading. At the water front, there is a large willow tree which had only hanging branches, but no leafs during winter (depicted in the right of Fig. 7). The corresponding point cloud map is shown in the middle (Oct. 10, 2013). Over the course of spring the willow tree grew more leaves and the corresponding point clouds became denser, which would have led to a very cluttered map. By detecting dynamic points, we are able to only use points for the final map, of which we are certain enough that they belong to a static structure. In Fig. 7, the points, which were classified as dynamic, are highlighted in yellow. At the example of the willow tree, we demonstrated both the importance of map maintenance, and the ability to readily use 3D mapping techniques to track environmental changes on shore.

5 Conclusion

In this article, we evaluated different types of filters aiming at a more accurate 3D state estimation in a context of shoreline monitoring with an ASV. Although building an accurate motion model of forces applied to a floating platform is not trivial, we demonstrated that filters using an approximated model provide better performance than filters without. Unfortunately, the simplicity of the model selected doesn't recover properly roll and pitch angles. Thus, we showed that adding the directly using IMU measurements and a complementary filter produces more accurate state estimates. Also, acceleration forces applied to a small or medium ASV are smaller than an UAV. In this application context, the combination of low accelerations and non-Gaussian noises on the GPS results in a wrong estimation of the IMU biases. This renders the use of IMU-centric

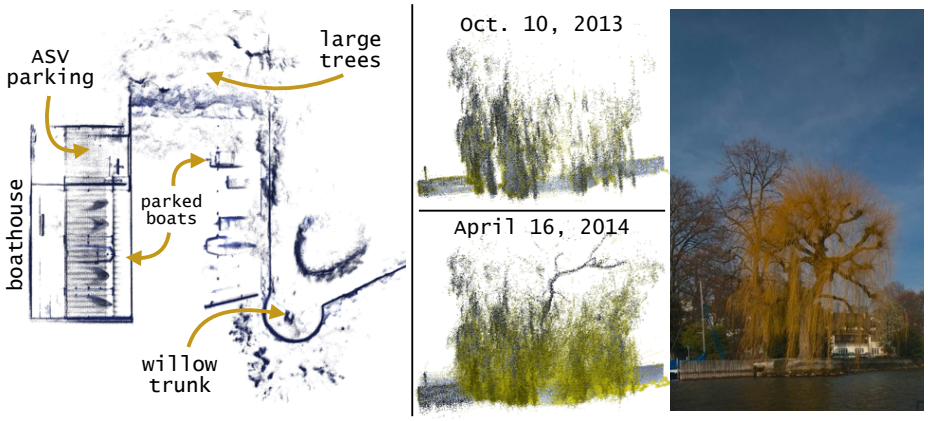

Fig. 7: Results of the shoreline mapping. *Left:* Top view of the resulting 3D point cloud map from combined data over 6 months. *Middle:* Side view of the willow tree, in October (Autumn) and April (Spring), respectively. *Right:* The willow tree in October.

filter less attractive in the case of an ASV. Moreover, GPS positions can have static offsets depending of the visible satellite constellations. This static bias can only be estimated by feeding another position sensor in the EKF. As we could highlight with our experimental setup, this offset causes a considerable error on all the solutions evaluated. Further research on how to handle this type of non-Gaussian GPS noise should be investigated in the future.

Acknowledgment This work was funded by the Swiss National Science Fund (CR22I2-130023) and the EU FP7 projects NIFTi (ICT-247870) and Tradr (ICT-609763). We also thank the Natural Sciences and Engineering Research Council of Canada (NSERC) and the *Fonds Québécois de la Recherche sur la Nature et les Technologies* (FQRNT) for the funds granted to Prof. P. Giguère.

Bibliography

[1] Bibuli, M., Bruzzone, G., Caccia, M., Lapierre, L.: Path-following Algorithms and Experiments for an Unmanned Surface Vehicle. Journal of Field Robotics 26(8), 669–688 (2009)

[2] Bosse, M., Zlot, R.: Continuous 3D scan-matching with a spinning 2D laser. In: 2009 IEEE International Conference on Robotics and Automation. pp. 4312–4319 (2009)

[3] Chen, V.L., Batalin, M.A., Kaiser, W.J., Sukhatme, G.: Towards Spatial and Semantic Mapping in Aquatic Environments. In: IEEE Int. Conf. on Robotics and Automation (ICRA). pp. 629–636 (2008)

[4] Dunbabin, M., Lang, B., Wood, B.: Vision-based Docking Using an Autonomous Surface Vehicle. In: IEEE Int. Conf. on Robotics and Automation (ICRA). pp. 26–32 (2008)

[5] Federal Office of Topography (swisstopo): Swiss map projections (May 18 2014), http://www.swisstopo.admin.ch/internet/swisstopo/en/home/topics/survey/sys/refsys/projections.html, [Online]
[6] Fossen, T.I.: Handbook of Marine Craft Hydrodynamics and Motion Control. Wiley, Chichester (2011)
[7] Grinham, A., Dunbabin, M., Gale, D., Udy, J.: Quantification of ebullitive and diffusive methane release to atmosphere from a water storage. Atmospheric Environment 45(39), 7166–7173 (2011)
[8] Hitz, G., Pomerleau, F., Garneau, M.E., Pradalier, C., Posch, T., Pernthaler, J., Siegwart, R.Y.: Autonomous Inland Water Monitoring: Design and Application of a Surface Vessel. Robotics & Automation Magazine, IEEE 19(1), 62–72 (2012)
[9] Kelly, J., Sibley, G., Barfoot, T., Newman, P.: Taking the Long View: A Report on Two Recent Workshops on Long-Term Autonomy. Robotics & Automation Magazine, IEEE 19(1), 109–111 (2012)
[10] Kitts, C., Mahacek, P., Adamek, T., Rasal, K., Howard, V., Li, S., Badaoui, A., Kirkwood, W., Wheat, G., Hulme, S.: Field operation of a robotic small waterplane area twin hull boat for shallow-water bathymetric characterization. Journal of Field Robotics 29(6), 924–938 (2012)
[11] Kubelka, V., Oswald, L., Pomerleau, F., Colas, F., Svoboda, T., Reinštein, M.: Robust Data Fusion of Multi-modal Sensory Information for Mobile Robots. Journal of Field Robotics (2014), to appear
[12] Leutenegger, S., Siegwart, R.Y.: A Low-Cost and Fail-Safe Inertial Navigation System for Airplanes. In: IEEE Int. Conf. on Robotics and Automation (ICRA). pp. 612–618 (2012)
[13] Mahony, R., Hamel, T., Pflimlin, J.: Nonlinear complementary filters on the special orthogonal group. Automatic Control, IEEE Transactions on 53(5), 1203–1218 (2008)
[14] Maimone, M., Cheng, Y., Matthies, L.: Two Years of Visual Odometry on the Mars Exploration Rovers. Journal of Field Robotics 24(3), 169–186 (2007)
[15] Michael, N., Shen, S., Mohta, K., Mulgaonkar, Y., Kumar, V., Nagatani, K., Okada, Y., Kiribayashi, S., Otake, K., Yoshida, K., Ohno, K., Takeuchi, E., Tadokoro, S.: Collaborative mapping of an earthquake-damaged building via ground and aerial robots. Journal of Field Robotics 29(5) (Sep 2012)
[16] Papadopoulos, G., Kurniawati, H., Sharif, A.S.B.M., Wong, L.J., Patrikalakis, N.M.: 3D-Surface Reconstruction for Partially Submerged Marine Structures Using an Autonomous Surface Vehicle. In: IEEE/RSJ Int. Conf. on Intelligent Robots and Systems (IROS). pp. 3551–3557 (2011)
[17] Pereira, A., Das, J., Sukhatme, G.: An experimental study of station keeping on an underactuated ASV. In: IEEE/RSJ Int. Conf. on Intelligent Robots and Systems (IROS). pp. 3164–3171 (2008)
[18] Pomerleau, F., Krüsi, P., Colas, F., Furgale, P., Siegwart, R.Y.: Long-term 3D map maintenance in dynamic environments. In: IEEE Int. Conf. on Robotics and Automation (ICRA) (2014), accepted
[19] Pomerleau, F., Colas, F., Siegwart, R., Magnenat, S.: Comparing ICP Variants on Real-World Data Sets. Autonomous Robots 34(3), 133–148 (2013)
[20] Scherer, S., Rehder, J., Achar, S., Cover, H., Chambers, A., Nuske, S., Singh, S.: River mapping from a flying robot: state estimation, river detection, and obstacle mapping. Autonomous Robots 33(1-2), 189–214 (2012)
[21] Trawny, N., Roumeliotis, S.I.: Indirect Kalman Filter for 3D Attitude Estimation A Tutorial for Quaternion Algebra. Tech. Rep. 612, University of Minnesota, Departement of Computing Science and Engineering (2005)